



# Potential Uses of Local Clay Materials for the Production of Porcelain Electrical Insulators, Ethiopia

Eshetu Bekele Wondemagegnehu · Tamirat Addis · Enyew Amare Zereffa · Andualem Merga Tullu · Belay Brehane · Lemma Teshome Tufa · Jaebeom Lee

Accepted: 1 June 2023 / Published online: 29 June 2023  
© The Author(s), under exclusive licence to The Clay Minerals Society 2023

**Abstract** Clays are extremely variable materials with different mineral compositions, and they are the main ingredients in ceramics applications. Their properties play specific roles in influencing the technological properties and performance of ceramics products. Evaluating the various properties can help to determine the best way to utilize clay materials, such as the locally available Bombawuha (BC) and Denkaka (DC) clays mined from Ethiopia's Bombawuha and Denkaka areas, respectively. The objective of this study was to examine these materials for the purpose of using them to produce quality electrical porcelain insulators. The clay samples were characterized for their chemical composition, mineralogy, thermal properties, plasticity, and particle-size distribution, using

atomic absorption spectrometry (AAS), X-ray diffraction (XRD), differential thermal analysis coupled with thermogravimetric analysis (DTA-TGA), the Atterberg plasticity test, and sieve hydrometer analysis. Based on the characteristics, suitable clay materials were selected and mixed with feldspar and quartz to formulate various porcelain body compositions which were fired at three different temperatures (1200, 1250, and 1300°C) and dwell times (1.5, 2.0, and 2.5 h). The mineralogy, water adsorption, apparent porosity, bulk density, dielectric strength, flexural strength, and microstructure of the fired bodies were measured. The results revealed that, compared to DC, BC contains kaolinite as the major mineral with appreciable amounts of silica (46.72 wt.%), alumina (35.32 wt.%), and fluxing oxides but smaller amounts of CaO. BC contains greater clay fractions (20.58 wt.%); and has a middle-range plasticity index (PI = 11.2 wt.%), thus making BC suitable for producing porcelain insulators. A test-body composition of 40 wt.% BC, 40 wt.% feldspar, and 20 wt.% quartz, fired at 1250°C for 2 h, exhibited water adsorption of 0.17 wt.%, apparent porosity of 0.42 wt.%, bulk density of 2.45 g/cm<sup>3</sup>, a dielectric strength of 8.22 kV/mm, and flexural strength of 43.63 MPa and, thus, satisfied the required properties for quality porcelain insulators.

Associate Editor: Prakash B. Malla

E. B. Wondemagegnehu (✉) · T. Addis · E. A. Zereffa · L. T. Tufa

Department of Applied Chemistry, School of Applied Natural Sciences, Adama Science and Technology University, PO Box 1888, Adama, Ethiopia  
e-mail: eshetubekele@gmail.com

A. M. Tullu  
Faculty of Chemistry, Silesian University of Technology, Marcina Strzody 9, 44-100 Gliwice, Poland

B. Brehane  
Department of Chemical Engineering, Adama Science and Technology University, P O Box, 1888 Adama, Ethiopia

L. T. Tufa · J. Lee  
Department of Chemistry Engineering and Applied Chemistry, Chungnam National University, Daejeon 34134, Republic of Korea

**Keywords** Clay · Firing time · Plasticity · Porcelain insulator · Sintering temperature

## Introduction

Porcelain electrical insulators are the most complex multi-phase ceramic materials produced from naturally available plastic materials (clay), fluxing agents

(feldspar), and filler materials (quartz) under various thermal conditions (Iqbal & Lee, 2000; Mehta et al., 2018; Nwachukwu & Lawal, 2018). It is a critical material in electric power-transmission and distribution systems primarily for two major functions: fastening mechanically and insulating the electrical network's component (Fadaeeasrami et al., 2022; Liebermann & Schulle, 2002). Raw materials play specific roles in influencing the technological properties and performance of the final products as well as decreasing processing costs by saving energy (Bragança & Bergmann, 2004; Locks et al., 2021; Olupot et al., 2010). The product is less sensitive to minor differences in the composition of raw materials, enabling the use of a wide range of clays. High mechanical and dielectric strength are essential properties of porcelain electrical insulators for outdoor applications (Ologunwa et al., 2021). Other crucial properties include low porosity and water adsorption. These depend on the properties of raw materials that may vary due to the geological condition of the original deposit, particle size, composition of the selected raw materials, and firing conditions (Bauluz et al., 2003; Velde & Meunier, 2008; Yaya et al., 2017).

The clay materials are mostly crystalline and distinguished by layered structures composed of polymeric sheets of  $\text{SiO}_4$  tetrahedra linked to sheets of  $(\text{Al}, \text{Mg}, \text{Fe})(\text{O}, \text{OH})_6$  octahedra (Al-Ani & Sarapää, 2008; Guggenheim et al., 1995). Clays are materials with various mineral compositions and are the main ingredients in ceramic processing; as a result, extensive studies have been made on clays and their applications (Gliozzo et al., 2014; Lahcen et al., 2014; Manni et al., 2017; Trindade et al., 2010). Ceramic applications of clay materials include bricks, fire-clay refractories, stoneware, porcelain insulators, sanitaryware, and tableware (Imagwuike et al., 2020). The utility of a clay mineral in ceramic applications is due to its physicochemical properties, mainly dependent on the arrangement and composition of the tetrahedral and octahedral sheets (Al-Ani & Sarapää, 2008; Baccour et al., 2009; Tsozué et al., 2017). Additional factors include particle-size distribution, plasticity, the non-clay mineral composition, organic-material content, the type and amount of exchangeable ions, soluble salts, and the clay texture (Gliozzo et al., 2014; Lahcen et al., 2014; Moraes et al., 2017; Trindade et al., 2010; Tsozué et al., 2017). Examining these properties can help to determine the best way to utilize clay materials.

In porcelain electrical insulators, clay provides plasticity for body forming, which binds the coarse particles of quartz and feldspar to maintain shape at the green stage (Kaviraj et al., 2021), and forms mullite during the firing process (Lee & Iqbal, 2001; Kitouni & Harabi, 2011). Clay minerals with weak interlayer forces and very fine particle sizes, e.g. montmorillonite and ball clays, adsorb a lot of water in the interlayer and belong in the upper range of plasticity. This kind of clay mineral has the potential to crack during fabrication (Akwilapo & Wiik, 2003). On the other hand, kaolinite and illite minerals have strong intermolecular attractive forces between the layers and exhibit moderate to low plasticity and can dry quickly, resulting in only slight shrinkage. As a result, kaolinite and illite are considered suitable for porcelain insulator fabrications (Valásková, 2015).

Mullite ( $3\text{Al}_2\text{O}_3 \cdot 2\text{SiO}_2$ ), which is formed when clay is fired at an elevated temperature, is the primary objective in the production of porcelain insulators, and it is a characteristic constituent of all ceramic microstructures (Islam et al., 2004; Meng et al., 2012; Merga et al., 2019). Porcelain microstructure consists of coarse quartz particles and mullite crystals embedded in a glassy phase (Ngayakamo & Park, 2018a). The formation of crystalline mullite, the particle size of the quartz, the viscosity of the glassy phase, and their homogeneity throughout the body of the microstructure have the potential to tune the ultimate properties of the porcelain insulator. Mullites, which have either a cuboid structure (primary mullites) or a needle-like, highly interlocked structure (secondary mullites), have various useful properties, such as low thermal expansion, a high melting point, high thermal stability, low dielectric constant, high thermal shock resistance, and chemical stability (Hossain et al., 2018; Sánchez-Soto et al., 2018). As a result, its formation improves a porcelain insulator's flexural strength and dielectric strength (Akwilapo & Wiik, 2003; Belhouchet et al., 2019; Ngayakamo & Eugene Park, 2019). Such properties of mullite can be controlled by adequate selection of clay minerals (Yaya et al., 2017). A significant alumina content or low  $\text{SiO}_2:\text{Al}_2\text{O}_3$  ratio in kaolinite or illite favor mullite formation. Due to the small alumina content in montmorillonite, mullite formation is less favored (Merga et al., 2019). Clay also contains small amounts of oxides, such as  $\text{Na}_2\text{O}$ ,  $\text{CaO}$ ,  $\text{MgO}$ ,  $\text{TiO}_2$ , and  $\text{Fe}_2\text{O}_3$  (Salihu & Suleiman, 2018), which may influence the

body's crystallization behavior, vitrification temperature, and glass viscosity (Iqbal & Lee, 2000). The presence of such oxides may reduce the compactness of the ceramic, inhibit mullite formation, maintain overall porosity at as much as 15 wt.% (Manfredini & Hanuskova, 2012), lead to a significant reduction in material strength, and deterioration of its dielectric property (Gao et al., 2015; Kyasager & Prasanna, 2016), and impart color (Manfredini & Hanuskova, 2012). Therefore, clay minerals having particular and appropriate characteristics are essential in order to obtain porcelain insulators with the required physical, electrical, and mechanical properties when fired with feldspar and quartz at high temperatures.

Despite the widespread availability of natural clay materials such as clay deposits in the Bombowha, Denkaka, and Kombolch areas of the Oromia region, as well as the clay found in the Belesa (Hosanna) and Ansho areas in the southern part of Ethiopia; their characteristics have been determined at a superficial level only (Ayele et al., 2016; Fentaw & Mengistu, 1998; Merga et al., 2019). Moreover, local ceramic production, which relies mainly on imported ball clay and locally available BC and DC, does not consider the chemical, mineralogical, and thermal characteristics of clay materials, thus contributing to the production of poor quality porcelain insulators and ceramic tiles in the country (Merga et al., 2019). A detailed study of the physicochemical properties, mineralogical composition, grain-size distributions of the local clay materials, firing time, temperature, and the fired bodies' characteristics is required. Therefore, the purpose of the present study was to investigate the aspects of locally available clay materials (specifically BC and DC) for use in producing quality porcelain electrical insulators.

## Materials and Methods

### Collection and Preparation of Raw Materials

The raw material samples collected and investigated as a potential clay source for porcelain electrical insulator production were Denkaka clay (DC) and Bombawuha clay (BC). They were mined initially from a deposit located at Bombawuha (6° 05' 20" N and 38° 46' 30" E) and Denkaka (8° 33' 36" N, 39° 10' 29" E) in Ethiopia. Chanco sand (CS), and a mixture of Wolkite

feldspar (WF) and Arerti feldspar (AF), of known composition and mineralogy, were used as a source of quartz and feldspar, respectively. Di Yuan Ceramics (Ethiopia) Plc, located in the Eastern Industrial Park, Dukem, Ethiopia, processed and supplied the samples. Clay samples were ground using a planetary ball mill (P100, FRETSCHE, Oberstein, Germany). Clays and feldspar were passed through a 63 µm sieve, while quartz was passed through a 45 µm sieve to homogenize and make them ready for further use (Mehta et al., 2018; Yaya et al., 2017).

### Characterization of Clay Samples

The clay samples were characterized for their chemical compositions, mineralogy, thermal properties, particle-size distributions, and plasticity. Their chemical compositions (oxide forms) were determined using Atomic Absorption Spectrometry (AAS model, spectra AA-20 plus, Varian Mulgrave, Victoria, Australia). Loss on ignition (LOI) was measured by the mass difference of samples heated at 105°C and 1000°C for 2 h (Jara et al., 2020; Regassa et al., 2014) at a laboratory of the geological survey of Ethiopia. The phase analysis of clay samples before and after calcination at 600°C for 2 h was carried out using a MAXima\_X XRD-7000 (Shimadzu, Tokyo, Japan) using CuK $\alpha$  radiation ( $\lambda = 1.5418 \text{ \AA}$ ), the accelerating voltage and filament current were maintained at 40 kV and 30 mA, respectively (Morkel & Vermaak, 2006). Samples were scanned over a Bragg angle range of 10 to 80°2 $\theta$ . The diffraction pattern was analyzed by search match against the International Center for Diffraction Database (ICDD) using the software *X'Pert High-Score Plus* (Iqbal, 2008). Thermal properties of clay samples were analyzed using a thermogravimetric analyzer (TGA) coupled with a differential thermal analyzer (DTA) (Shimadzu DTG-60H, Japan). The sample was heated in a platinum cup from ambient temperature to 1200°C at a rate of 10°C/min, while an empty platinum cup served as a control (Mahmoudi et al., 2016). Plasticity parameters, i.e. the Atterberg limits [liquid limit (LL), plastic limit (PL), and plastic index (PI)] of clay samples were measured by the Casagrande method according to ASTM D4318-10 (2005). The hydrometer test determined the particle-size distribution of clays finer than 75 µm and those coarser than 75 µm by wet sieve analysis according to ASTM D422-63 (2007).

## Porcelain Electrical Insulator Bodies; Formulations, and Design of Experiments

An experiment was designed to determine the effect of selected clay material on porcelain insulator body properties (physical, electrical, and mechanical) at various firing temperatures and for various dwell times. Accordingly, three formulations of porcelain electrical insulator bodies based on the work of Merga et al. (2019), denoted Batch-1, Batch-2, and Batch-3 (Table 1) were prepared in triplicate using BC, which possessed better chemical, mineralogical, plasticity, and particle-size properties than DC. In the formulations, feldspars (WF+AF) were used mainly as a source of alkaline oxides to produce a low-viscosity liquid phase. Quartz (CS) as a filler, upon dissolution to a glass phase, increased the strength of the porcelain body. The formulations were ball milled for 6 h with 7 wt.% water to make them suitable for dry pressing. A cylindrical shape, 80 mm in diameter and 5 mm thick, was prepared from each batch by dry pressing to determine water adsorption and dielectric strength. A rectangular porcelain electrical insulator body of dimension 75 mm×38 mm×7 mm was prepared using a selected batch (with good electrical properties) to determine flexural strength. Samples of the electrical insulator bodies were allowed to dry at room temperature and then fired at three temperatures, 1200, 1250, and 1300°C, for 1.5 h, 2 h, and 2.5 h at a heating rate and cooling rate of 10°C/min (Gaied et al., 2011; Merga et al., 2019).

### Characterization of Porcelain Electrical Insulators

Physical properties (water adsorption, apparent porosity, and bulk density) of porcelain electrical

**Table 1** Formulation of porcelain electrical insulator samples (wt.%)

	Formulation		
	Batch-1	Batch-2	Batch-3
Clay (BC)	50	45	40
Quartz	10	15	20
Feldspar	40	40	40

BC: Bombawuha Clay

insulator fired bodies were determined using the boiling method according to ASTM C373-88 (1999). Dielectric strength was measured using a high-voltage testing machine (model TERCO HV 11039103, STOCKHOLM, SWEDEN) by evaluating their breakdown voltage. They are calculated as follows:

$$\text{Water adsorption (wt.\%)} = \frac{W_s - W_d}{W_d} \times 100 \quad (1)$$

$$\text{Apparent Porosity (wt.\%)} = \frac{W_s - W_d}{W_s - W_{sp}} \times 100 \quad (2)$$

$$\text{Bulk density (g/mL)} = \frac{W_d}{W_s - W_{sp}} \quad (3)$$

$$\text{Dielectric strength (kV/mm)} = \frac{\text{breakdown voltage (kV)}}{\text{thickness of the sample (mm)}} \quad (4)$$

where:  $W_s$  = soaked weight,  $W_d$  = dry weight,  $W_{sp}$  = suspended weight.

The flexural strength was determined according to the three-point loading method (ASTM D790-17, 2002) using a flexural breaking load machine (model MOR 5-TS/185, SASSUOLO, ITALY) at the Ethiopian Conformity Assessment Enterprise Laboratory. The flexural strength by the three-point test was calculated as follows:

$$\text{Flexural strength (MPa)} = 3FL/2WD^2 \quad (5)$$

where:  $F$  is the maximum force applied,  $L$  is the length of the sample,  $W$  is the width of the sample, and  $D$  is the depth of the sample.

Scanning electron microscopy coupled with energy dispersive X-ray spectroscopy (SEM-EDS) was carried out using a field emission scanning electron microscope (COXEM Co.,Ltd, Daejeon, South Korea equipped with *Quantax 70* software for elemental analysis (EDS) (Bruker Nano GmbH, Berlin, Germany) to determine the microstructure and elemental composition of fired samples. The results were supplemented by the quantitative chemical analysis of the surfaces of the solid samples using an X-ray photoelectron Spectrometry (XPS) (Thermo Scientific, Seoul, South Korea) with micro-focused monochromatic  $AlK\alpha$  X-ray radiation ( $h\nu = 1350$  eV).

## Results and Discussion

### Characteristics of the Raw Materials

#### Chemical Compositions

The chemical compositions and ‘loss on ignition’ (LOI) of the clay materials used (Table 2) showed that the oxides in both BC and DC are composed mainly of silica (46.72 wt.% for BC and 47.90 wt.% for DC) and alumina (35.32 wt.% for BC and 27.84 wt.% for DC), with a small percentage of other oxides such as iron oxides and fluxing oxides. The ratios of the principal oxides ( $\text{SiO}_2/\text{Al}_2\text{O}_3$ ) for BC and DC were ~1.3 and 1.7, respectively, which indicated that BC is much closer to pure kaolinite (1.18) (Mahmoudi et al., 2016). The greater ratio of the principal oxides ( $\text{SiO}_2/\text{Al}_2\text{O}_3$ ) in DC than in BC indicated a higher level of quartz in DC than in BC (Ghorbel et al., 2008; Mahmoudi et al., 2016). The amount of CaO is very large in DC (5.54 wt.%) compared to that in BC (0.74 wt.%) (Table 2); this is associated with the appreciable amount of calcite in DC (Lahcen et al., 2014). The result suggested that more gases may form during sintering, which may cause cracks in the fired bodies, leading to high porosity and water adsorption in the porcelain insulator bodies prepared from DC (Aghayev & Küçükuysal, 2018). Alkaline oxides ( $\text{K}_2\text{O}$  and  $\text{Na}_2\text{O}$ ) that act as fluxing materials are more prominent in BC (1.62 wt.%) than in DC (0.46 wt.%). The LOI values of BC (13.85 wt.%) and DC (13.41 wt.%) were comparable with classical kaolinitic clays (14 wt.%), related mainly to the presence of clay minerals, hydroxides, and organic matter (Faria & Holanda, 2013; Tsozué et al., 2017). In both clays, the amounts of color-forming oxide,  $\text{Fe}_2\text{O}_3$ , and fluxing oxides,  $\text{K}_2\text{O} + \text{Na}_2\text{O}$ , were less than those reported by Gliozzo et al. (2014), Lahcen et al. (2014); Manni et al. (2017), and Trindade et al. (2010) in various clay types. This was attributed to the samples being less weathered, as confirmed by the greater

intensity of quartz and vermiculite and the absence of feldspars and illite minerals in the XRD pattern (Manni et al., 2017).

The results confirmed that the clay material was kaolinite. However, the relative purity of BC (which has a ratio for  $\text{SiO}_2/\text{Al}_2\text{O}_3$  close to that of pure kaolin), the small amount of CaO, and the large amount of alkaline oxide present make BC much more suitable for the fabrication of electrical porcelain insulators than DC. The ratio of  $\text{SiO}_2/\text{Al}_2\text{O}_3$  in BC was notable for mullite-phase formation during the sintering of the porcelain body (Gralik et al., 2014; Olupot et al., 2010; Zbik et al., 2010). Moreover, the amounts of color-forming impurities,  $\text{Fe}_2\text{O}_3$  and  $\text{TiO}_2$ , in the clay materials were within the standard requirement for porcelain insulator production and could serve to enhance the action of flux, causing melting to start at lower temperatures with more abundant liquid phases (Andreev & Zakharov, 2009; Gaied et al., 2011; Souza et al., 2011; Tang et al., 2012). The amount of alkaline oxides ( $\text{K}_2\text{O}$  and  $\text{Na}_2\text{O}$ ) in BC was (1.62 wt.%), which is comparable with commonly used china clay (Huber Corporation, 1955) and greater than in ball clay (Carty & Senapati, 1998). Even though the amounts of these fluxing agents are small, they may still contribute to reduction of the sintering temperature.

#### Mineralogical Composition

The XRD patterns of BC and DC powders, untreated and following heat treatment at 600°C, are shown in Fig. 1. Untreated BC indicated the presence of kaolinite (ICDD Card No: 01-080-0885), quartz (ICDD Card No: 01-083-0539), gibbsite (ICDD Card No: 01-070-2038), and microcline (ICDD Card No: 01-076-1238) (Fig. 1). Similarly, the pattern of DC showed kaolinite (ICDD Card No: 01-080-0886), quartz (ICDD Card No: 01-086-1560), and alunite (ICDD Card No: 00-014-0136) (Fig. 1). The peak intensities in the XRD patterns

**Table 2** Chemical compositions and loss on ignition values (LOI) (wt.%) of the two clay materials

Clay Materials	Oxides												
	$\text{SiO}_2$	$\text{Al}_2\text{O}_3$	$\text{Fe}_2\text{O}_3$	CaO	MgO	$\text{Na}_2\text{O}$	$\text{K}_2\text{O}$	MnO	$\text{P}_2\text{O}_5$	$\text{TiO}_2$	$\text{H}_2\text{O}$	LOI	Si/Al
BC	46.72	35.32	0.83	0.74	0.16	0.54	1.08	<0.01	0.20	0.13	1.76	13.85	1.16
DC	47.90	27.84	0.32	5.54	0.18	Trace	0.46	Trace	0.05	0.33	3.50	13.41	1.51

BC Bombawuha clay, DC Denkaka clay, Trace = <0.1, and LOI = Loss on ignition

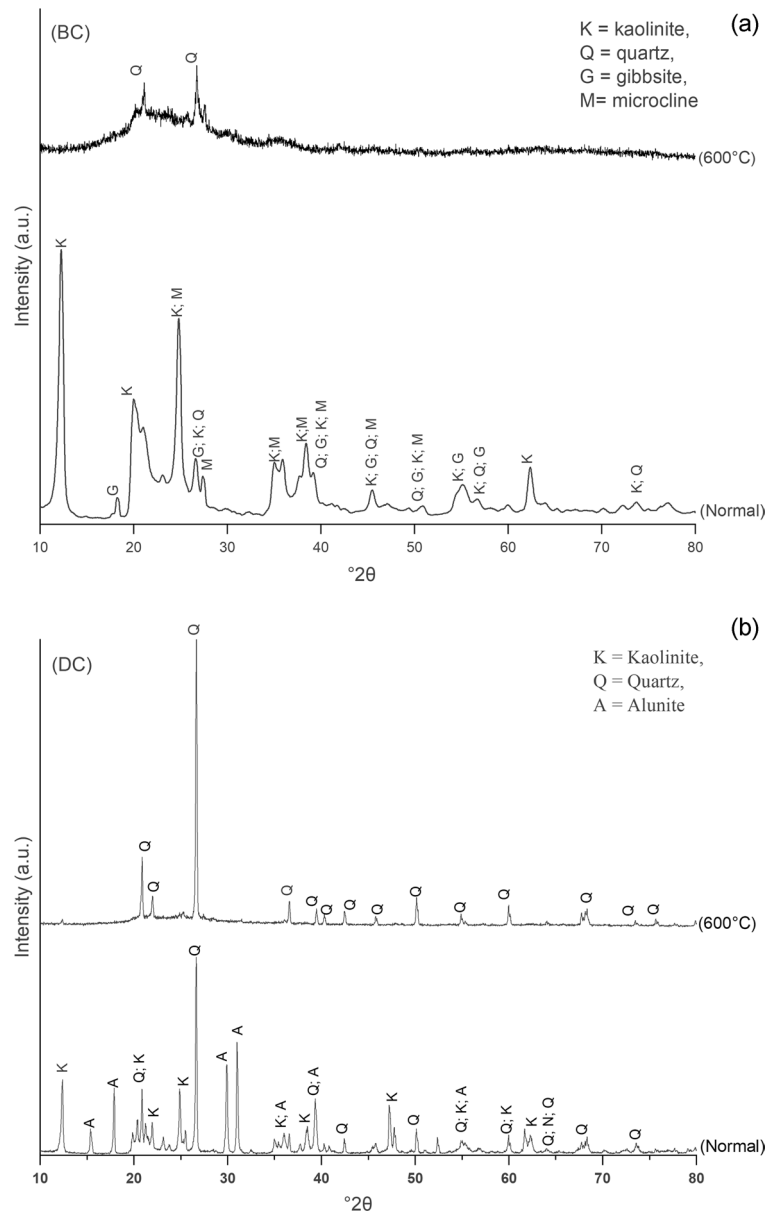


**Fig. 1** Powder XRD patterns of untreated clay and after heat treatment at 600°C of: **a** Bombowha clay (BC) and **b** Denkaka clay (DC)

indicated that BC contained kaolinite as the primary crystalline phase and the non-clay minerals quartz, microcline, and gibbsite as the minor phases. In comparison, the XRD pattern of DC was characterized by kaolinite and quartz as the primary phase and alunite as the minor phase. The disappearance of the diffraction peaks of kaolinite and the appearance of amorphous aluminosilicate, especially for BC after calcination at 600°C (Fig. 1), confirmed

further the presence of the kaolinite phase, which was transformed to metakaolinite by loss of the hydroxide groups above 450°C and leaving quartz intact (Iqbal & Lee, 2000; Brindley & Nakahira, 2006; Merga et al., 2019). The observed diffraction peaks, which were more intense in the XRD pattern of DC after calcination at 600°C, are due to the quartz, which remained intact (Ayele et al., 2016). In general, this mineralogical composition is typical

of clays of this region (Merga et al., 2019). Several authors have also reported the presence of major mineral phases: quartz, vermiculite, illite, kaolinite, smectite, and calcite in clay deposits in Africa (Gliozzo et al., 2014; Lahcen et al., 2014; Trindade et al., 2010; Tsozué et al., 2017). The XRD patterns of BC and DC agreed with the chemical analysis results obtained from AAS, in which BC had more

kaolin minerals and less quartz than DC, resulting in a smaller  $\text{SiO}_2/\text{Al}_2\text{O}_3$  ratio for BC (1.32) than for DC (1.72) (Table 2). Thus, BC is the preferred clay mineral for production of quality porcelain insulators as it has the required amount of alumina for mullite-phase formation during sintering of the porcelain body, and the quartz content present can also be dissolved easily by vitreous flow during firing.

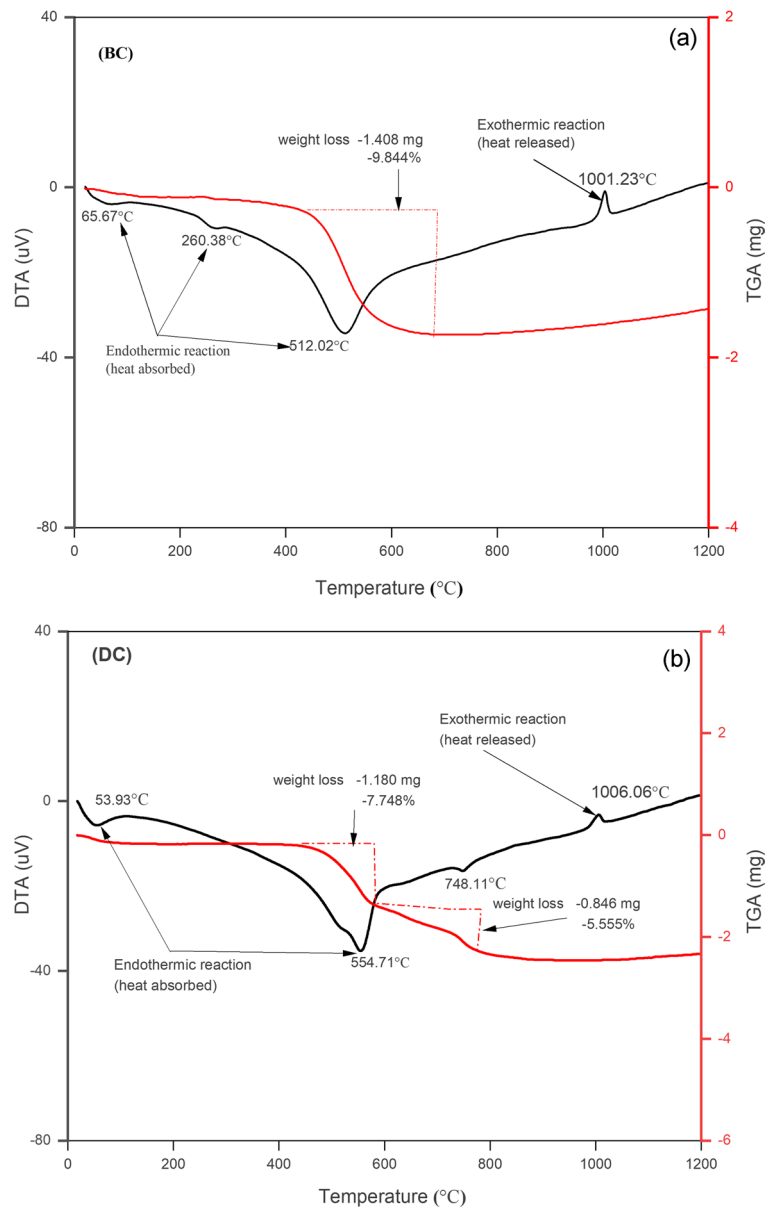


**Fig. 2** Differential thermal analysis (DTA) and thermogravimetric analysis (TGA) of: **a** Bombawuha clay (BC) and **b** Dankaka clay (DC)

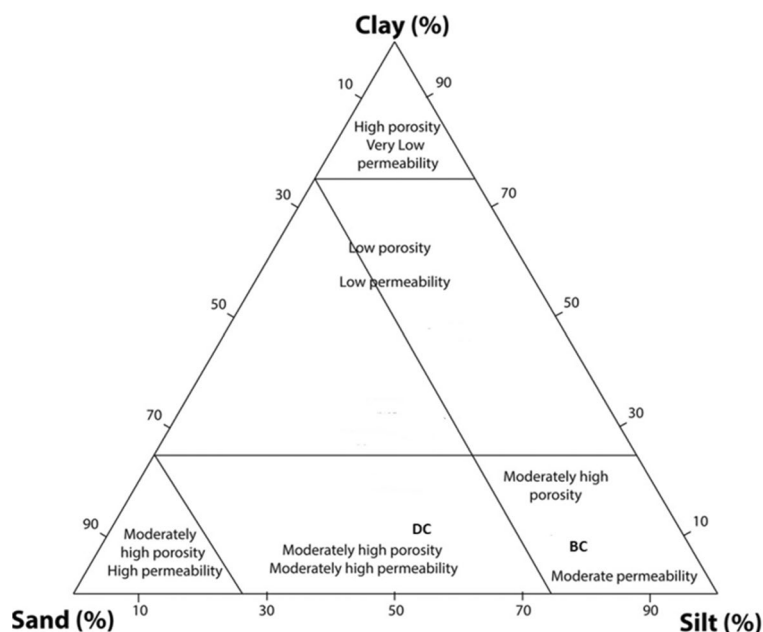
**Table 3** Particle-size distribution (wt.%) of Bombawuha clay (BC) and Dankaka clay (DC)

Particle-size distribution	Clay types	
	BC	DC
<0.002 mm (clay fraction)	20.50	12.17
0.075–0.002 mm (silt fraction)	79.11	56.03
4.75–0.075 mm (sand fraction)	0.39	31.8

### Thermal Properties

TGA-DTA thermograms of BC and DC are shown in Fig. 2. As shown in the DTA curve, the endothermic peak at 65.67°C for BC and at 53.93°C for DC was attributed to the removal of weakly bound water of clay minerals (Bennour et al., 2015; Holanda, 2012; Manni et al., 2017), and the mass loss associated with this peak was ~1 wt.% for both clays (Fig. 2). The weak endothermic valley at 260.38°C for BC could be related to the transformation of the free gibbsite sheet (Gaied et al., 2011; Mercury et al., 2011). The broad endothermic bands centered at 512.02°C for BC and at 554.71°C for DC are within a characteristic temperature range (420 to 660°C) for metakaolin-phase formation as a result of the dehydroxylation

of kaolinite, and an  $\alpha \rightarrow \beta$ -quartz transformation (Heide & Földvari, 2006; Ghorbel et al., 2008; Iqbal & Lee, 2000; Yaya et al., 2017). Quartz transformation was more pronounced for DC as it contains more quartz (Lahcen et al., 2014; Manni et al., 2017). The observed mass loss in the TGA curve associated with the endothermic peak was 9.84 wt.% and 7.75 wt.% for BC and DC, respectively (Fig. 2). This was due mainly to the loss of the structural hydroxide groups upon structural rearrangement of the octahedral sheet of kaolinite ( $\text{Al}_2\text{O}_3 \cdot 2\text{SiO}_2 \cdot 2\text{H}_2\text{O}$ ) to a tetrahedral configuration in metakaolin ( $2\text{SiO}_2 \cdot \text{Al}_2\text{O}_3$ ) at the specified temperature range (Ghorbel et al., 2008; Iqbal & Lee, 2000; Krupa & Malinarič, 2015). The observed difference between BC and DC is consistent with the idea that clay minerals with a low  $\text{Al}_2\text{O}_3/\text{SiO}_2$  ratio (higher kaolinite degree) tend to form a large amount of a metakaolin phase, and, at the same time, lose a large amount of structural hydroxide (Lahcen et al., 2014). The small endothermic peak at 748.11°C for DC was attributed to the decomposition of calcite into CaO (Bennour et al., 2015; Çelik, 2017; Lahcen et al., 2014). The associated weight loss of 5.5 wt.% agreed with the observed chemical analysis (Table 2). A more intense exothermic peak observed at 1001.23°C for BC compared to the observed

**Fig. 3** Ternary diagram of the clay sediments studied following the relationship between the sand, silt, and clay fractions and their controls over porosity and permeability



**Table 4** Liquid limit (LL), plastic limit (PL), and plasticity index (PI) of BC and DC

Atterberg limit tests	BC (wt.%)	DC (wt.%)
Liquid limit (LL)	32	21.7
Plastic limit (PL)	20.8	17.5
Plastic index (PI)	11.3	4.2

BC Bombawuha clay, DC Denkaka clay

exothermic peak at 1006.06°C for DC was due to the formation of mullite.

### Particle-Size Distribution

The particle-size distributions (sand, silt, and clay fractions) of BC and DC are summarized in Table 3. The results showed that the percentages of clay fractions (<0.002 mm particle size) were ~20.6 wt.% for BC and ~12.7 wt.% for DC; the silt fractions (0.075–0.002 mm particle size range) were ~79.11 wt.% for BC and 56.03 wt.% for DC; the sand fractions (4.75–0.075 mm particle size range) were ~0.39 wt.% for BC and 31.8 wt.% for DC (Table 3). The particle-size results, specifically the percentage of clay fractions obtained for both BC and DC, showed variations in most clay samples (GlioZZo et al., 2014; Lahcen et al., 2014; Trindade

et al., 2010; Tsozué et al., 2017). The result confirmed variation in particle size between BC and DC. BC contains a greater proportion of clay-fraction material than did DC; accordingly, it has greater plasticity. The large silt fractions in both BC and DC indicate the need for pre-treatment, such as crushing and sieving, before use in ceramics manufacture, e.g. as porcelain insulators (Trindade et al., 2010). The greatest sand content in DC may facilitate drying and contribute to the formation of the glassy phase during sintering; as a result, it would improve the mechanical strength in ceramics manufacture (Lahcen et al., 2014). According to the ternary diagram of McManus (1988), which describes the relationship between sand, silt, and clay fractions with their controls over porosity and permeability (Fig. 3), the results of particle-size analysis of the BC sample fell in the moderately high porosity and moderate permeability, and, for the DC sample, fell under the moderately high porosity and moderately high permeability region.

### Plasticity

The plasticity test results of BC and DC (Table 4) showed that the liquid limits (LL) were 32 wt.% for BC and 21.7 wt.% for DC, while the plastic limits (PL)

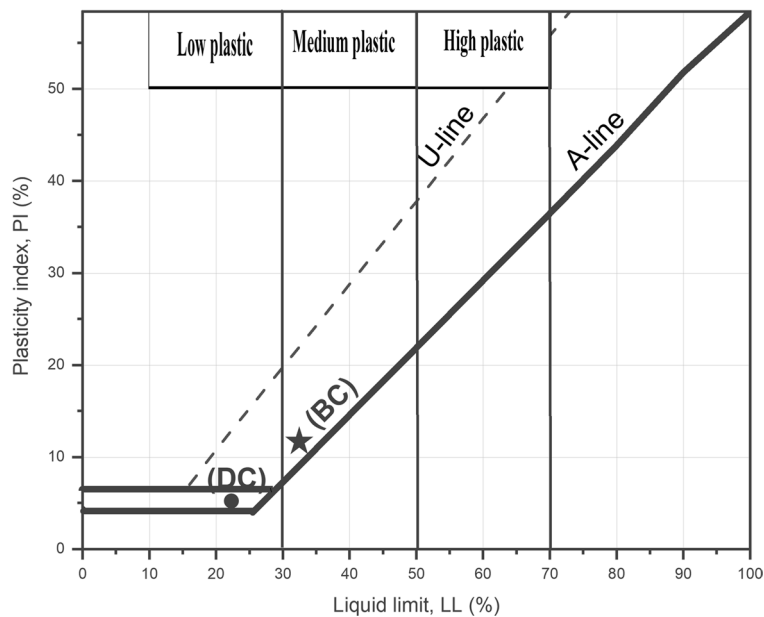


**Fig. 4** Positions of the Bombawuha clay (BC) and Dankaka clay (DC) on the Holtz and Kovacs plasticity chart

were 20.8 and 17.5 wt.% for BC and DC, respectively. Based on the Atterberg limits, the plasticity indexes, PI (determined by the formula  $PI = LL - PL$ ;  $LL$  = liquid limit;  $PL$  = plastic limit) were 11.2 wt.% for BC and 4.2 wt.% for DC (Table 4). The observed PI implies that BC is characterized by the middle range of plasticity ( $7 \text{ wt.}\% < PI < 17 \text{ wt.}\%$ ), and DC exhibits a low range of plasticity ( $PI < 7 \text{ wt.}\%$ ) according to the Atterberg classification (Roy & Kumar Bhalla, 2017). The higher PI of BC than DC was due to the presence of a greater clay fraction ( $< 2 \mu\text{m}$ ) in BC (Table 3, Fig. 1). The PI of clay increases linearly with the percentage of the clay-sized fraction (Lahcen et al., 2014; Laskar & Pal, 2012). Even though the observed PI results of both clay materials were smaller than commonly used china clay and ball clay (Carty & Senapati, 1998), slight variations were also observed with PI values of various clay types reported by others (Lahcen et al., 2014; Trindade et al., 2010; Tsozué et al., 2017). This is due to the presence of the major non-clay impurities, quartz, and other minor impurities, as shown in Table 2, as well as geological formations and particle-size distribution (Lahcen et al., 2014), which can impact significantly the plasticity of a porcelain body. Similar to most clay samples, the calculated consistency limits for BC (Fig. 4) were in the medium plastic region, while DC is located in a low plastic region (Holtz et al., 2013). Moreover, the results revealed that the clay materials might not need much quartz material in the formulation to decrease plasticity (Bennour et al., 2015; Gaied et al., 2011). This ensures that the plasticity value of BC is suitable and encourages optimal behavior in pressing and drying (negligible contraction and easy to dry) during production of porcelain electrical insulators. In comparison, the PI of DC implied that the sample was not appropriate for making porcelain electrical insulators due to the risk of cracking and increased thermal conductivity (Manni et al., 2017; Tsozué et al., 2017).

#### Characteristics of Fired Porcelain Electrical Insulators

##### *Water Adsorption*

Water adsorption of the three formulations (Batch-1, Batch-2, and Batch-3) fired at various temperatures and for various durations of time are shown in Fig. 5a–c. The water adsorption, which indicates the

amount of open pores and the size of the fired bodies, decreased as the firing temperature increased and reached a minimum of  $1300^\circ\text{C}$  for all firing times. The percentage of water adsorption of batches increased in the order Batch-3 < Batch-2 < Batch-1 at an optimized firing temperature of  $1250^\circ\text{C}$  and firing time of 2 h (Fig. 5b). This coincided with the level of  $\text{SiO}_2$  in the batch compositions, where a larger  $\text{SiO}_2$  content was accompanied by a smaller percentage of water adsorption (Batch-3). In porcelain bodies,  $\text{SiO}_2$  with a grain size of  $< 45 \mu\text{m}$  is dissolved in the feldspathic glassy phase to fill the gaps or voids in the microstructure leading to less water adsorption by the porcelain body (Carty & Senapati, 1998; Figueirêdo et al., 2019; Iqbal & Lee, 2000; Kimambo, 2014). Generally, the batch compositions containing more  $\text{SiO}_2$  (Batch-2 and Batch-3) and fired at an optimum firing temperature of  $1250^\circ\text{C}$  and firing time of 2.0 h had water adsorption values which fulfill the standard requirement for porcelain electrical insulators, i.e. water adsorption  $< 0.5 \text{ wt.}\%$  (Ngayakamo & Eugene Park, 2019).

##### *Apparent Porosity*

A porcelain insulator needs to be fired for a time and temperature which give the minimum value, usually zero or close to zero, of the apparent porosity (Kimambo, 2014). Like water adsorption, the apparent porosity decreased as the firing temperature increased and reached a minimum at  $1300^\circ\text{C}$  (Fig. 6a–c). At the specified temperature, the smallest percent porosity was obtained for Batch-3 compared to other batches at all firing times, indicating the dissolution of more silica into the glass phase and the formation of sufficient vitreous phase to fill the pores (Ghorbel et al., 2008; Martín-Márquez et al., 2009). Batch-3 attained a minimum value of the apparent porosity (0.42 wt.%) at an optimum firing temperature of  $1250^\circ\text{C}$  and time of 2 h. The result confirmed that the apparent porosity depended on the relative proportion of  $\text{SiO}_2$  added to the porcelain insulator and the firing temperature (between 1250 and  $1300^\circ\text{C}$ ) at which the vitreous phase enabled minimum porosity.

##### *Bulk Density*

The variations in bulk density (BD) as a function of temperature with various dwell times are shown in

Fig. 7a–c. No significant change was noted in the bulk density of the porcelain bodies sintered at various firing temperatures and times. All test samples showed greater degrees of densification independent of their composition. This is due to the promotion of viscous liquid formation associated with the presence of minerals such as microcline and the absence of free quartz from the porcelain body (Martín-Márquez et al., 2009; Schettino et al., 2016).

In general, Batch-2 and Batch-3 fired at the optimum temperature of 1250°C for 2 h had better physical properties that met the standard requirement for porcelain electrical insulators than Batch-1, i.e. water adsorption < 0.5 wt.%, less apparent porosity, and bulk density (> 1.71 g/cm<sup>3</sup>) (Ngayakamo & Park, 2018b). These batch compositions fulfilled the requirement for water adsorption, apparent porosity, and bulk density with better physical properties at a firing temperature of 1300°C than at a firing temperature of 1250°C. This is due mainly to progressive dissolution and the conversion of more SiO<sub>2</sub> to a glassy phase which fills the void spaces to enable less water adsorption with increasing firing temperature (Benhour et al., 2015; Mehta et al., 2018; Ochen, 2019). From an economic perspective, however, using a lower firing temperature is better for saving energy and production costs.

### *X-Ray Diffractograms*

X-ray diffractograms of porcelain insulator samples fired for 2 h (which possess better physical properties) as a function of firing temperature (1250 and 1300°C) are shown in Fig. 8a–c. Mullite and quartz were the primary crystalline phases identified in all fired samples. Mullite is a product of metakaolinite transformation or subsequent reaction of metakaolinite with feldspar at higher temperatures, and quartz is a residual mineral of the raw materials used (Schettino et al., 2016). The XRD patterns of Batch-1 (Fig. 8a) showed a significant reduction in the intensity of quartz peaks as the temperature increased, indicating that firing at 1300°C led to the dissolution of more quartz into the glass phase with a slight change in the mullite content (Gralik et al., 2014; Martín-Márquez et al., 2009). The relative intensity of quartz is greatest in Batch-2. It showed a slight decrease with temperature (Fig. 8b). The XRD patterns of the fired bodies of Batch-3 showed no significant change in the peak intensity for

quartz and mullite with an increased firing temperature (Fig. 8c). The peaks of quartz in Batch-2 may indicate a large amount of free quartz in the composition. This facilitated the free movement of mobile ions such as Na<sup>+</sup>, K<sup>+</sup>, and Al<sup>3+</sup>; as a result, the dielectric strength of the porcelain insulators may be smaller (Belhouchet et al., 2019). This confirms that increasing the temperature beyond 1250°C may be necessary to improve the porcelain insulator quality of Batch-2; but may not be necessary to improve the porcelain insulator quality of batch-3 as it did not enhance/affect mullite formation and porcelain microstructure quartz composition.

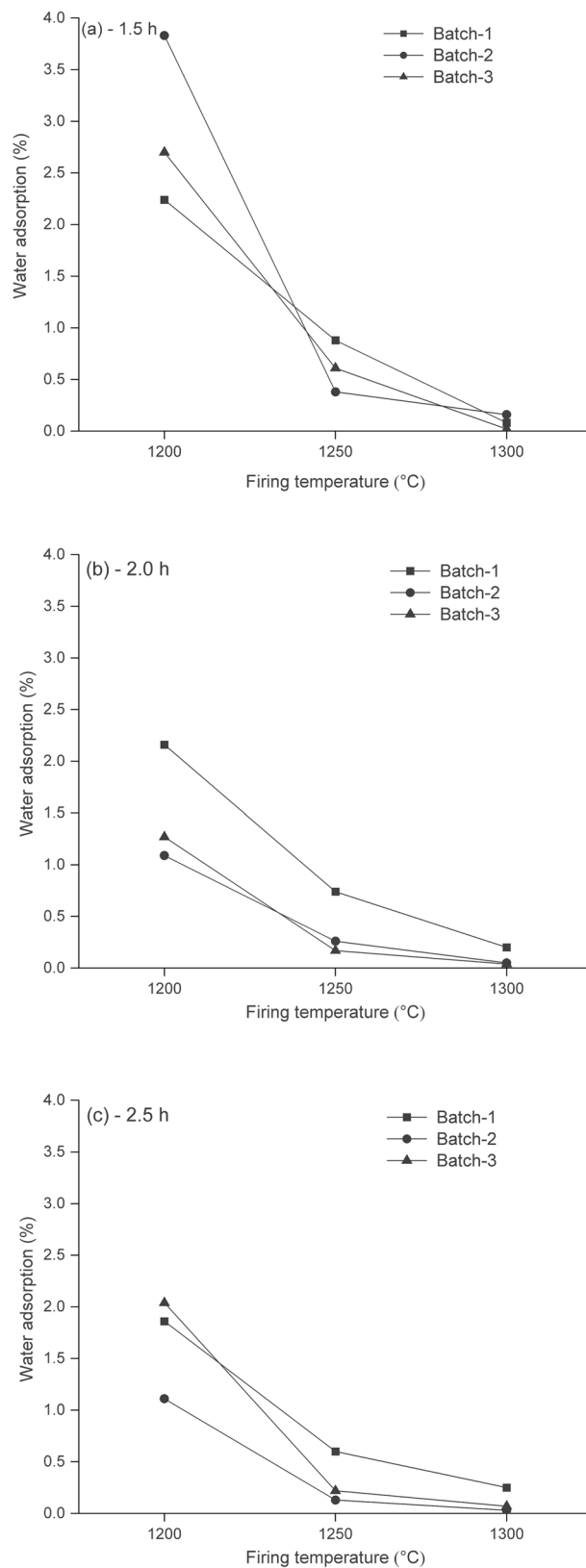
### *Dielectric Strength*

Dielectric strength is an essential property of ceramic insulators, and the dielectric strength of the fired bodies is shown in Fig. 9a–c. The dielectric strength of all the batches increased with firing temperature and reached a maximum at 1300°C for all firing times. This is associated with the amount of secondary mullite or glassy phase that contributes to densification and the dissolution of more SiO<sub>2</sub> into the glass phase which fills up the pores (Ghorbel et al., 2008; Iqbal & Lee 2000). The dielectric strength values obtained at a firing temperature of 1300°C and dwell time of 1.5 h for Batch-1 (11.37 kV/mm) was the greatest of all the samples (Fig. 9a), in which the large amounts of mullite phase may have contributed to the observed result. On the other hand, the free quartz in the fired bodies of Batch-2 may have contributed to the smallest observed dielectric strength of the porcelain insulators (Fig. 9a–c). Dielectric strength values at the optimized firing temperature and firing time (1250°C, 2 h) were greatest for Batch-3 (8.22 kV/mm) (Fig. 9b), and fulfilled the specified range (6.1–13 kV/mm) for porcelain insulators (Olupot et al., 2010). The observed value of Batch-3 at the optimized temperature and time was associated with sufficient liquid-phase formation and the level of dissolved silica in the mixture that fills up the pores, resulting in increased dielectric strength of the porcelain insulator (Ngayakamo & Eugene Park, 2019; Islam et al., 2004; Kitouni, 2014).

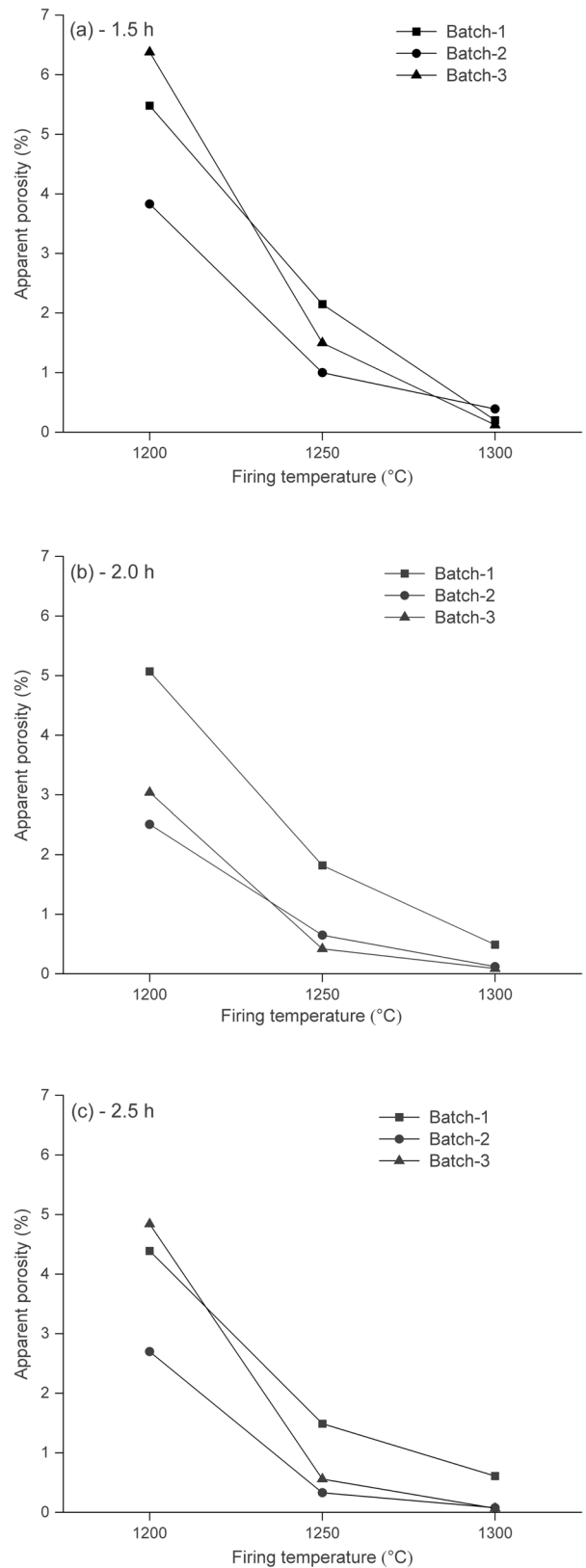
### *Flexural Strength/Modulus of Rupture (MOR)*

The flexural strength of selected porcelain insulators with better physical and electrical properties are shown in Fig. 10. The flexural strength for the batches

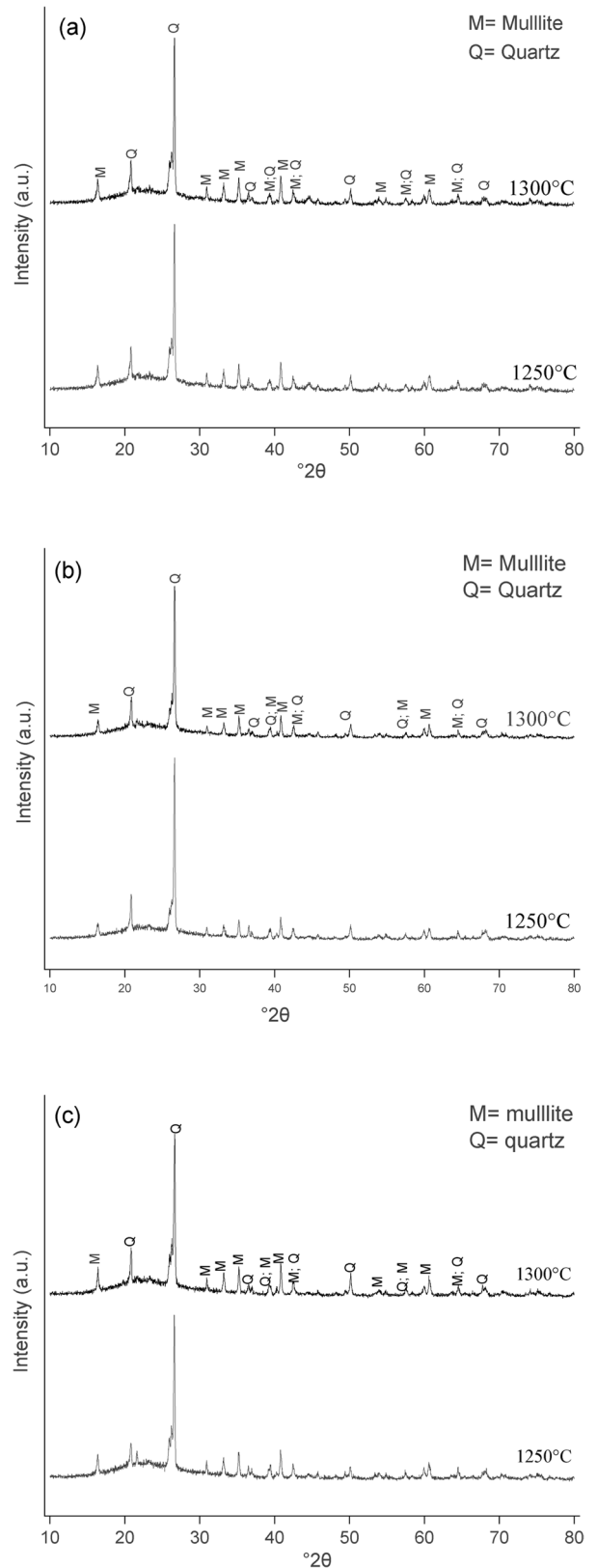
**Fig. 5** Water adsorption of porcelain insulators (Batch-1, Batch-2, Batch-3) at various firing temperatures (1200, 1250, and 1300°C) and firing times of **a** 1.5 h, **b** 2.0 h, and **c** 2.5 h



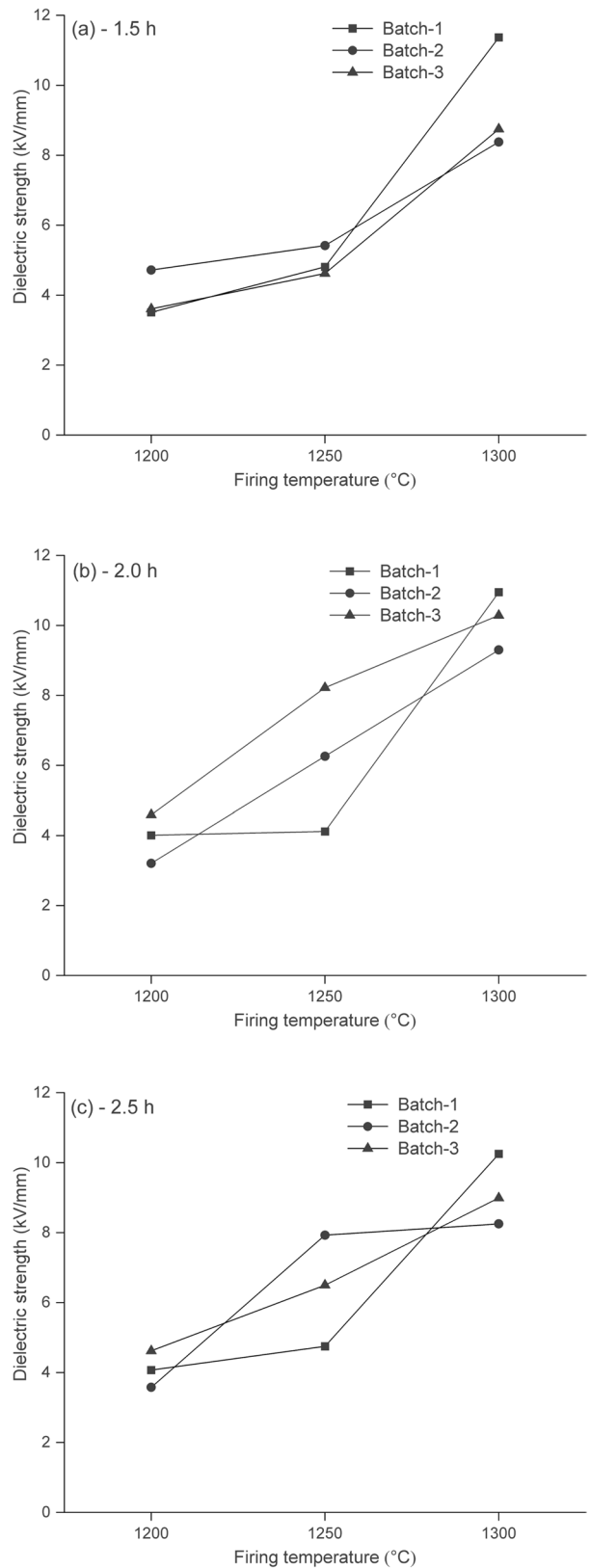
**Fig 6** Apparent porosity of porcelain insulators (Batch-1, Batch-2, Batch-3) at various firing temperatures (1200, 1250, and 1300°C) and firing times of **a** 1.5 h, **b** 2.0 h, and **c** 2.5 h



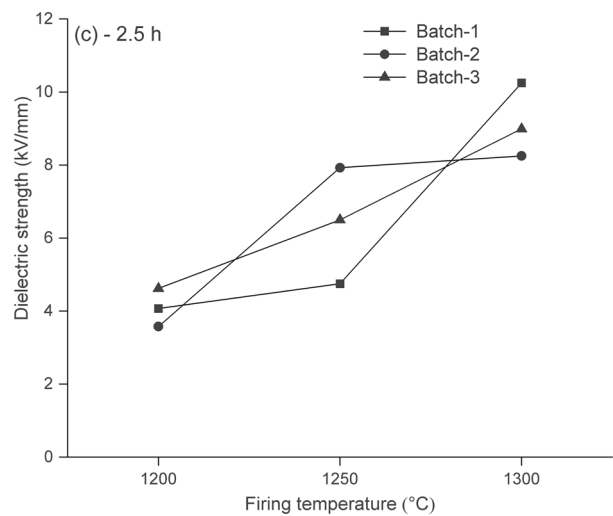
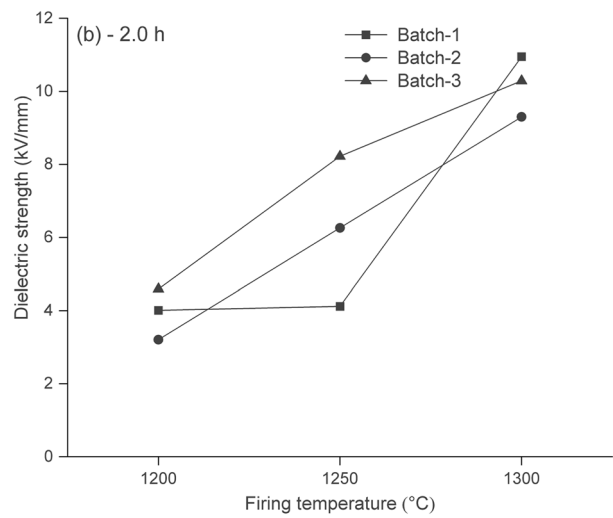
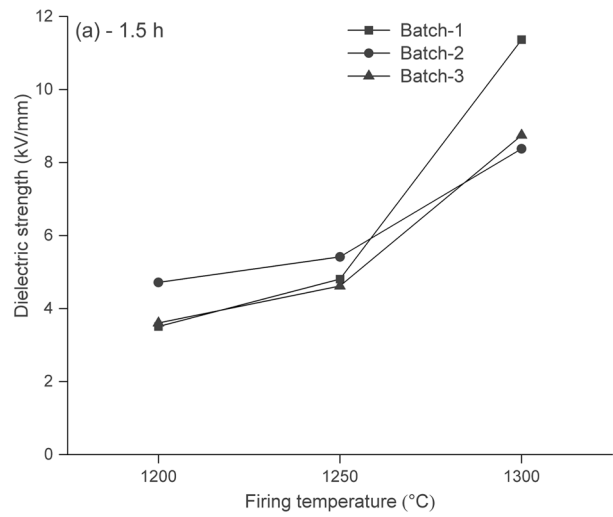
**Fig 7** Bulk density of porcelain insulators (Batch-1, Batch-2, Batch-3) at various firing temperatures (1200, 1250, and 1300°C) and firing time of **a** 1.5 h, **b** 2.0 h, and **c** 2.5 h



**Fig 8** XRD patterns of selected porcelain insulator samples fired at 1250 and 1300°C for 2 h: **a** Batch-1, **b** Batch-2, and **c** Batch-3



**Fig. 9** Dielectric strength (kV/mm) of porcelain insulators (Batch-1, Batch-2, Batch-3) at various firing temperatures (1200, 1250, and 1300°C) and firing times of **a** 1.5 h, **b** 2.0 h, and **c** 2.5 h





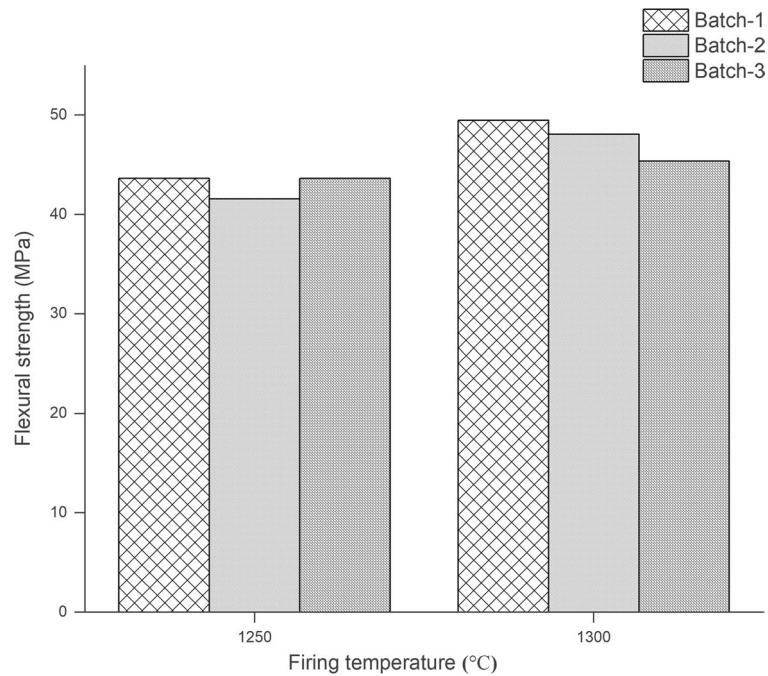


**Fig. 10** The flexural strength/modulus of rupture (MOR) of selected porcelain insulators as a function of firing temperature (1250 and 1300°C) for 2 h

at a firing temperature of 1250°C and dwell time of 2 h ranged between 41.58 and 43.64 MPa and met the standard requirement for porcelain insulators, i.e. >35 MPa (Ngayakamo & Eugene Park, 2019). This is associated with the amount of liquid or glassy phase that cements all the surrounding constituents together to decrease pore structure, and a small amount of free quartz in the porcelain microstructure results in

interconnected matrix fractures (Carty & Senapati, 1998; Darweesh, 2019). The greatest observed flexural strength for Batch-1 (49.48 MPa) at 1300°C can be explained by the increased amount of kaolinite transformed to mullite with firing temperature and the presence of less free quartz that does not influence the interconnected matrix as seen in the XRD pattern (Ghorbel et al., 2008; Teixeira et al., 2008; Souza et al., 2011).

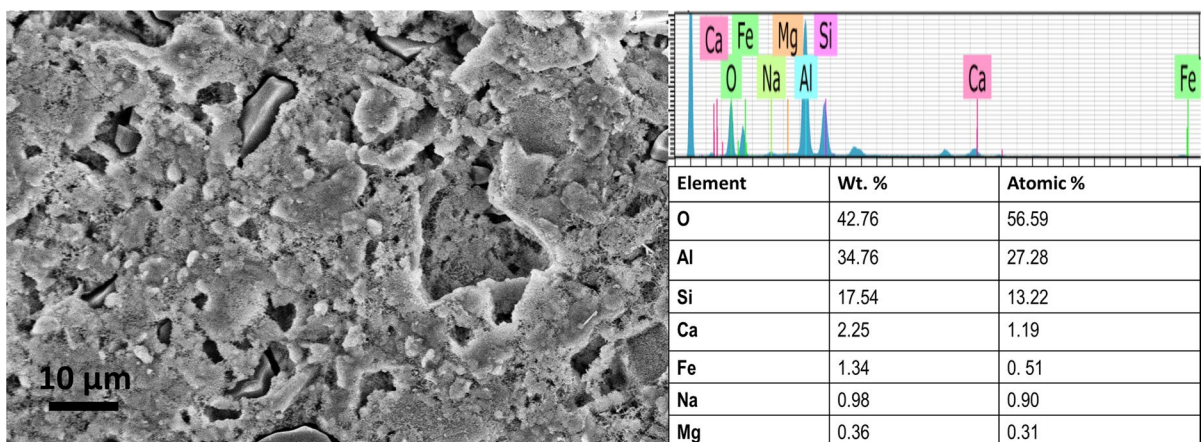


**Fig. 11** SEM image with corresponding EDS of fracture surfaces of Batch-3 fired at 1250°C for 2.0 h

### Surface properties

The SEM images and the corresponding EDS of Batch-3, which possesses better physical, electrical, and mechanical properties at the optimized firing temperature of 1250°C and dwell time of 2 h, are shown in Fig. 11. The micrographs in Batch-3 showed interconnected mullite phase and quartz particles of various sizes embedded in the glassy phase. This is a characteristic of porcelain microstructure (Ngayakamo & Park, 2018a). The quartz grain was retained from the raw materials as a result of partial sintering (Belhouchet et al., 2019), the reaction of metakaolinite with relics of feldspar formed the mullite phase, and the glassy phase was formed from feldspar melt (Iqbal & Lee, 2000; Meng et al., 2012; Merga et al., 2019). Similar photomicrographs were reported by Martín-Márquez et al. (2009) and Belhouchet et al. (2019).

The corresponding EDS mapping showed clearly the presence of all the targeted elements (O, Al, Si, Ca, Na, and Fe) distributed throughout the microstructure (Fig. 11). Moreover, the decrease in the molar ratio of Si/Al in the final product compared to the ratio in the clay materials (Table 2) confirmed the formation of the mullite phase as its formation was always accompanied by the liberation of the amorphous silica, thereby increasing the total amount of aluminum (Andreev & Zakharov, 2009; Carty & Senapati, 1998).

The XPS analysis was carried out to provide additional details on the surface properties of porcelain insulator samples. A wide-scan survey XPS profile (Batch-3) of the sample porcelain insulator body (Fig. 12a) revealed major peaks at 529.08 eV for O1s, 75.20 eV for Al2p, 103.08 eV for Si2p, 497.08 eV for Na1s, 294.08 eV for K2p, 351.06 eV for Ca2p, 711.08 eV for Fe2p, and 284.8 eV for C1s (the reference

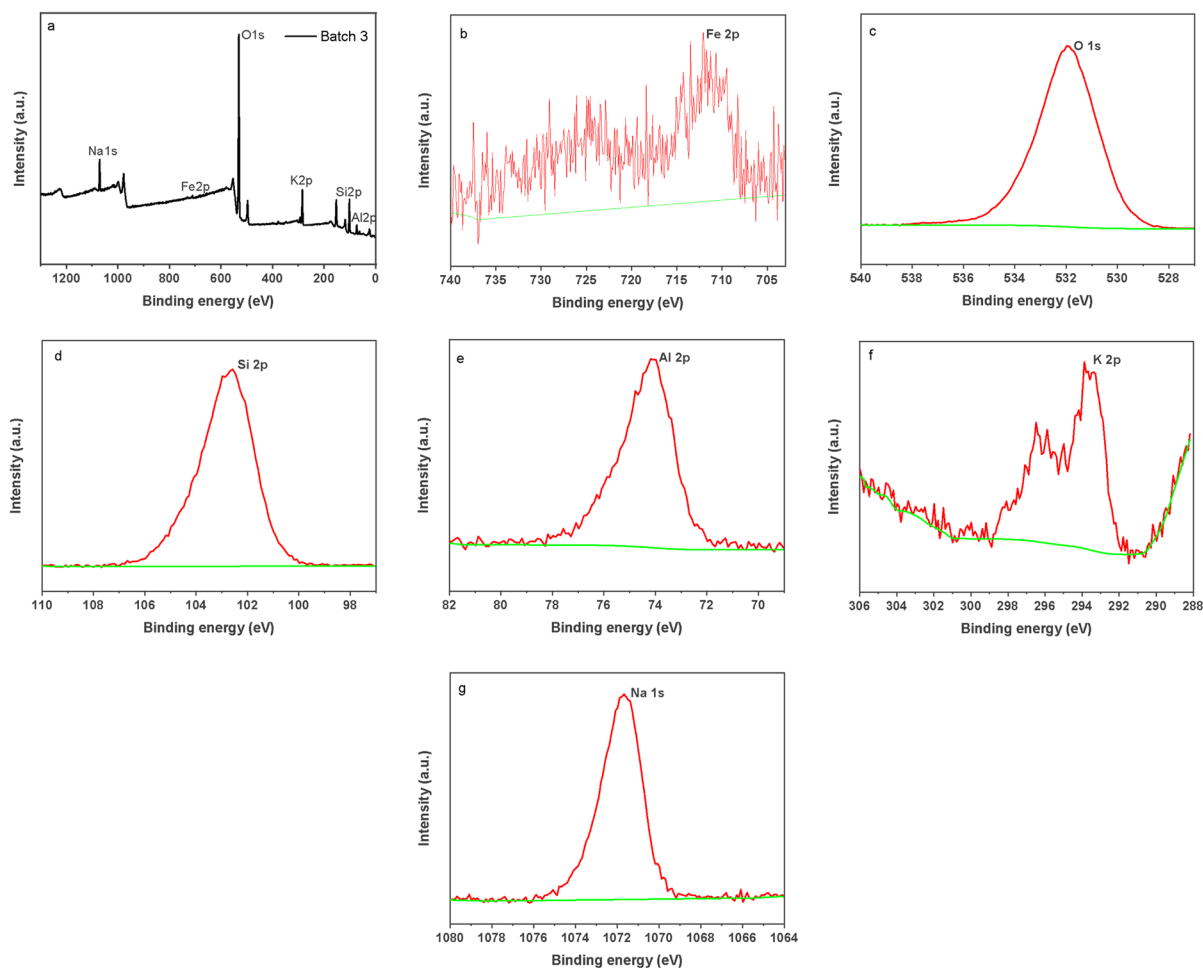


**Fig. 12** XPS profile of a sample porcelain insulator body (Batch-3)

binding energies). Furthermore, the profile displayed core level bands of Fe2p, O1s, Si2p, Al2p, K2p, and Na1s (Fig. 12b–g), consistent with the chemical composition analysis and EDS analysis results.

## Conclusions

The viability and prospects of the future existence of a manufacturing industry depend on the development or use of raw materials available locally. To this end, the current study investigated two locally available clay materials for their potential to produce quality porcelain electrical insulators. The analytical results of the clay materials and porcelain electrical insulator samples confirmed that BC deposits contain raw materials of suitable chemical composition to make porcelain electrical insulators. DC does not. The ratio of  $\text{SiO}_2/\text{Al}_2\text{O}_3$  in BC is close to that of pure kaolin and promotes mullite-phase formation during sintering. The intense exothermic peak observed at 1001.23°C for BC compared to the exothermic peak at 1006.06°C for DC in the DTA curve confirmed this. The principal mineral phases in both BC and DC were kaolinite and quartz. The quartz content in BC can be dissolved easily by the liquid phase formed during firing, however. To make DC suitable for the production of ceramics, adding more plastic clays to enhance its plasticity and compensate for the high level of quartz for effective digestion on firing would be necessary. Moreover, the higher level of CaO and quartz in DC required pre-treatment to reduce the quantity and size which may cause cracks in the fired bodies. The smaller amounts of fluxing oxides,  $\text{K}_2\text{O} + \text{Na}_2\text{O}$ , in both clay samples compared to other reported clay materials, mean that a feldspar which contains enough of these oxides is needed, otherwise greater proportions of feldspar will be needed to produce more quality porcelain electrical insulators.

The results confirmed that producing quality porcelain electrical insulators is possible using an appropriate mixture of clay, feldspar, and quartz at optimized conditions from locally available clay resources deposited in the Bombamuha area, Oromia region, Ethiopia. Batch 3, which contains BC (40 wt.%), quartz (20 wt.%), and feldspar (40 wt.%), and which was fired at 1250°C for 2 h, provided optimum mullite and crystalline quartz, which, embedded in a sufficient glassy phase, formed a dense microstructure as characterized

by XRD phase analysis and SEM-EDS. These methods gave values for water adsorption of 0.17 wt.%, apparent porosity of 0.42 wt.%, bulk density of 2.45 g/cm<sup>3</sup>, dielectric strength of 8.22 kV/mm, and flexural strength of 43.63 MPa, which meet the required standard for quality porcelain electrical insulators. Though better physical, electrical, and mechanical properties were obtained on firing at 1300°C, from an economic perspective, using a lower firing temperature and less time are preferred, to save energy and production costs.

Further study should consider the possible ways of minimizing major impurities in these clays. Optimization of the quartz size and amount in the clay materials is also needed as these factors have been found to be significant in determining the rates of dissolution and quartz transformation during sintering. These would have a significant impact on the two most important properties of a porcelain electrical insulator body, the dielectric and flexural strength. Further investigation is also needed into the use of clay materials for other ceramic ware which does not consider the dielectric strength, e.g. ceramic floor and wall tiles, as all of the present batch compositions meet the requirements of flexural strength (modulus of rupture) (>35 MPa) for ceramic wares.

**Acknowledgments** The authors acknowledge the financial support of the Adama Science and Technology University for this project. The authors give special thanks to the institutes supporting the laboratory analysis: Addis Ababa University, Department of Electrical Engineering; De-Yuan Ceramics Industry; Ethiopian Geological Survey; Ethiopian Conformity Assessment Enterprise; Chungnam National University, Chemistry Core Facility (Daejeon, South Korea).

**Funding** Adama Science and Technology University supported the research work.

**Data Availability** All data generated during this study are included in this research article.

**Code Availability (Software Application or Custom Code)** Not applicable.

## Declarations

**Conflict of Interest** On behalf of all authors, the corresponding author states that there are no conflicts of interest.

**Declaration of Interests** The authors declare that they have no known competing financial interests or personal relationships that could have appeared to influence the work reported in this paper.

## References

- Aghayev, T., & Küçükuysal, C. (2018). Ceramic properties of Uşak clay in comparison with Ukrainian clay. *Clay Minerals*, 53(4), 549–562. <https://doi.org/10.1180/clm.2018.40>
- Akwilapo, L. D., & Wiik, K. (2003). Ceramic properties of Pugu kaolin clays. Part I: Porosity and modulus of rupture. *Bulletin of the Chemical Society of Ethiopia*, 17(2), 147–154. <https://doi.org/10.4314/bcse.v17i2.61661>
- Al-Ani, T., & Sarapää, O. (2008). Clay and clay mineralogy. *Geochemical Survey of Finland*, 2008, 1–94.
- Andreev, D. V., & Zakharov, A. I. (2009). Ceramic item deformation during firing : Effect of composition and microstructure ( review ). *Refractories and Industrial Ceramics*, 50(4), 298–303. <https://doi.org/10.1007/s11148-009-9191-y>
- ASTM C373-88. (1999). Standard test method for water absorption, bulk density, apparent porosity, and apparent specific gravity of fired Whiteware products. *ASTM C373-88*, 88(reapproved), 1–2.
- ASTM D422. (2007). Standard test method for particle-size analysis of soils. *Astm, D422-63* (Reapproved), 1–8.
- ASTM D4318-10. (2005). Standard test methods for liquid limit, plastic limit, and plasticity index of soils. *Report*, 04(March 2010), 1–14.
- ASTM D790-17 (2002). Standard Test Methods for Flexural Properties of Unreinforced and Reinforced Plastics and Electrical Insulating Materials. D790. *Annual Book of ASTM Standards. i*: 1–12.
- Ayele, L., Pérez-Pariente, J., Chebude, Y., & Diaz, I. (2016). Synthesis of zeolite a using kaolin from Ethiopia and its application in detergents. *New Journal of Chemistry*, 40(4), 3440–3446. <https://doi.org/10.1039/c5nj03097h>
- Baccour, H., Medhioub, M., Jamoussi, F., & Mhiri, T. (2009). Influence of firing temperature on the ceramic properties of Triassic clays from Tunisia. *Journal of Materials Processing Technology*, 209(6), 2812–2817. <https://doi.org/10.1016/j.jmatprotec.2008.06.055>
- Bauluz, B., Mayayo, M. J., Fernández-Nieto, C., Cultrone, G., & González López, J. M. (2003). Assessment of technological properties of calcareous and non-calcareous clays used for the brick-making industry of Zaragoza (Spain). *Applied Clay Science*, 24(1), 121–126. [https://doi.org/10.1016/S0169-1317\(03\)00152-2](https://doi.org/10.1016/S0169-1317(03)00152-2)
- Belhouchet, K., Bayadi, A., Belhouchet, H., & Romero, M. (2019). Improvement of mechanical and dielectric properties of porcelain insulators using economic raw materials. *Boletín de La Sociedad Española de Cerámica y Vidrio*, 58(1), 28–37. <https://doi.org/10.1016/j.bsecv.2018.05.004>
- Bennour, A., Mahmoudi, S., Srasra, E., Hatira, N., Bousen, S., Ouaja, M., & Zargouni, F. (2015). Identification and traditional ceramic application of clays from the Chouamekh region in South-Eastern Tunisia. *Applied Clay Science*, 118, 212–220. <https://doi.org/10.1016/j.clay.2015.09.018>
- Bragança, S., & Bergmann, C. (2004). Traditional and glass powder porcelain: Technical and microstructure analysis. *Journal of the European Ceramic Society*, 24, 2383–2388. <https://doi.org/10.1016/j.jeurceramsoc.2003.08.003>
- Brindley, G., & Nakahira, M. (2006). The kaolinite-mullite reaction series: II, Metakaolin. *Journal of the American Ceramic Society*, 42, 314–318.
- Carty, W., & Senapati, U. (1998). Porcelain—Raw materials, processing, phase evolution, and mechanical behavior. *Journal of the American Ceramic Society*, 81, 3–20.
- Çelik, H. (2017). Technological characterization and comparison of two ceramic clays used for manufacturing of traditional ceramic products in Turkey. *Scientific Mining Journal*, 56(4), 137–147.
- Darweesh, H. H. M. (2019). Recycling of glass waste in ceramics — part I : physical , mechanical and thermal properties. *SN Applied Sciences*, 1(10), 1–11. <https://doi.org/10.1007/s42452-019-1304-8>
- Fadaeasrami, H., Faghihi, F., Olamaei, J., & Mohammadnezhadshourkaei, H. (2022). FEM analysis of polluted 230 kV porcelain insulators by introducing new asymmetrical contamination: Elliptical ring-shaped. *International Journal of Electrical Power & Energy Systems*, 142, 108274. <https://doi.org/10.1016/j.ijepes.2022.108274>
- Faria, K., & Holanda, J. (2013). Incorporation of sugarcane bagasse ash waste as an alternative raw material for red ceramic. *Cerâmica*, 59, 473–480. <https://doi.org/10.1590/S0366-69132013000300019>
- Fentaw, H. M., & Mengistu, T. (1998). *Comparison of Kombecha and Bombowha kaolins of Ethiopia* (pp. 149–164). Applied Clay Science.
- Figueirêdo, J., Silva, J., Neves, G., Ferreira, H., & Santana, L. (2019). Influence of processing variables on clay-based ceramic formulations. *Materials Research*, 22, 1–9. <https://doi.org/10.1590/1980-5373-MR-2018-0548>
- Gaied, M. E., Gallala, W., Essefi, E., & Montacer, M. (2011). Microstructural and mechanical properties in traditional ceramics as a function of Quartzofeldspathic sand incorporation. *Transactions of the Indian Ceramic Society*, 70(4), 207–214. <https://doi.org/10.1080/0371750X.2011.10600170>
- Gao, S., Liu, Y., Zhu, M. X., Tao, F. B., Zhou, Z. C., Bo, B., & Huang, Y. J. (2015). Study on operating properties of ceramic long rod insulator for transmission line. *Materials Research Innovations*, 19(January), S570–S575. <https://doi.org/10.1179/1432891715Z.0000000001327>
- Ghorbel, A., Fourati, M., & Bouaziz, J. (2008). Microstructural evolution and phase transformation of different sintered kaolins powder compacts. *Materials Chemistry and Physics*, 112(3), 876–885. <https://doi.org/10.1016/j.matchemphys.2008.06.047>
- Gliozzo, E., Iacoviello, F., & Foresi, L. M. (2014). Geosources for ceramic production: The clays from the Neogene-quadernary Albegna Basin (southern Tuscany). *Applied Clay Science*, 91–92, 105–116. <https://doi.org/10.1016/j.clay.2014.01.012>
- Gralik, G., Chinelatto, A. L., & Chinelatto, A. S. A. (2014). Effect of different sources of alumina on the microstructure and mechanical properties of the triaxial porcelain. *Cerâmica*, 60(356), 471–481. <https://doi.org/10.1590/S0366-69132014000400004>
- Guggenheim, S., Martin, R. T., Alietti, A., Drits, V. A., Formoso, M. L. L., Galán, E., Köster, H. M., Morgan, D. J., Paquet, H., Watanabe, T., Bain, D. C., Ferrell, R. E., Bish, D. L., Fanning, D. S., Guggenheim, S., Kodama, H., & Wicks, F. J. (1995). Definition of clay and clay mineral: Joint report of the AIPEA nomenclature and

- CMS nomenclature committees. *Clays and Clay Minerals*, 43(2), 255–256.
- Heide, K., & Földvari, M. (2006). High temperature mass spectrometric gas-release studies of kaolinite  $\text{Al}_2[\text{Si}_2\text{O}_5(\text{OH})_4]$  decomposition. *Thermochimica Acta*, 446(1–2), 106–112. <https://doi.org/10.1016/j.tca.2006.05.011>
- Holanda, K. C. P. F. J. N. F. (2012). Thermal study of clay ceramic pastes containing sugarcane bagasse ash waste. *Journal of Thermal Analysis and Calorimetry*, 1–6. <https://doi.org/10.1007/s10973-012-2878-11>
- Holtz, R. D., Kovacs, W. D., & Sheahan, T. C. (2013). *An introduction to geotechnical engineering*. Dorling Kindersley India Pvt.
- Hossain, S. K. S., Mathur, L., Roy, P. K., Hossain, S. K. S., Mathur, L., & Rice, P. K. R. (2018). Rice husk/rice husk ash as an alternative source of silica in ceramics: A review. *Journal of Asian Ceramic Societies*, 6(4), 299–313. <https://doi.org/10.1080/21870764.2018.1539210>
- Imagwuike, I. M., Nduka, N. B., Anthony, O. I., & Chibundo, N. P. (2020). Development of standard formulations for porcelain production from Ohiya clay. *Kathmandu University Journal of Science, Engineering and Technology*, 15(1), 1–10.
- Iqbal, Y. (2008). On the glassy phase in tri-axial porcelain bodies. *Journal of Pakistan Materials Society*, 2(2), 62–71.
- Iqbal, Y., & Lee, W. E. (2000). Microstructural evolution in tri-axial porcelain. *Journal of the American Ceramic Society*, 83(12), 3121–3127. <https://doi.org/10.1111/j.1151-2916.2000.tb01692.x>
- Islam, R. A., Chan, Y. C., & Islam, M. F. (2004). Structure-property relationship in high-tension ceramic insulator fired at high temperature. *Materials Science and Engineering B: Solid-State Materials for Advanced Technology*, 106(2), 132–140. <https://doi.org/10.1016/j.mseb.2003.09.005>
- Huber Corporation (1955). *Kaolin clays and their industrial uses*. J.M. Huber Corporation, Edison, New Jersey, USA.
- Jara, A. D., Woldetinsae, G., Betemariam, A., & Kim, J. Y. (2020). Mineralogical and petrographic analysis on the flake graphite ore from Saba Boru area in Ethiopia. *International Journal of Mining Science and Technology*, 30(5), 715–721. <https://doi.org/10.1016/j.ijmst.2020.05.025>
- Kaviraj, A. K., Saha, S., Chakraborty, A., Pahari, G., Ray, D., Parya, T. K., & Das, S. K. (2021). Differences in phase, microstructural, and electrical characteristics of quartz-substituted alumina porcelain insulator. *Journal of the Australian Ceramic Society*, 57(2), 327–337. <https://doi.org/10.1007/s41779-020-00535-4>
- Kimambo, V. (2014). Suitability of Tanzanian kaolin, quartz and feldspar as raw materials for the production of porcelain tiles. *International Journal of Science, Technology and Society*, 2, 201. <https://doi.org/10.11648/j.ijsts.20140206.17>
- Kitouni, S. (2014). Dielectric properties of Triaxial porcelain prepared using raw native materials without any additions. *Balkan Journal of Electrical and Computer Engineering*, 2(3), 128–131.
- Kitouni, S., & Harabi, A. (2011). Sintering and mechanical properties of porcelains prepared from Algerian raw materials. *Ceramica*, 57(344), 453–460. <https://doi.org/10.1590/S0366-69132011000400013>
- Krupa, P., & Malinarič, S. (2015). Thermal properties of green alumina porcelain. *Ceramics International*, 41(2), 3254–3258. <https://doi.org/10.1016/j.ceramint.2014.11.015>
- Kyasager, S. B., & Prasanna, N. D. (2016). Development of optimum slip ratio for high voltage porcelain insulator manufacturing. *International Research Journal of Engineering and Technology*, 03(02), 522–527.
- Lahcen, D., Hicham, E. E., Latifa, S., Abderrahmane, A., Jamal, B., Mohamed, W., Meriam, E., & Nathalie, F. (2014). Characteristics and ceramic properties of clayey materials from Amezmitz region (Western high atlas, Morocco). *Applied Clay Science*, 102, 139–147. <https://doi.org/10.1016/j.clay.2014.09.029>
- Laskar, A., & Pal, S. K. (2012). Geotechnical characteristics of two different soils and their mixture and relationships between parameters. *Electronic Journal of Geotechnical Engineering*, 17 U(2004), 2821–2832.
- Lee, W. E., & Iqbal, Y. (2001). Influence of mixing on mullite formation in porcelain. *Journal of the European Ceramic Society*, 21, 2583–2586. [https://doi.org/10.1016/S0955-2219\(01\)00274-6](https://doi.org/10.1016/S0955-2219(01)00274-6)
- Liebermann, J., & Schulle, W. (2002). Bauxite porcelain: A new high-tech product for high-voltage insulation. *American Ceramic Society Bulletin*, 81, 33–38.
- Locks, M., Arcaro, S., Bergmann, C. P., Ribeiro, M. J. P. M. J., Raupp-Pereira, F., & Montedo, O. R. K. (2021). Effect of feldspar substitution by basalt on pyroplastic behaviour of porcelain tile composition. *Materials*, 14(14), 10.3390/ma14143990.
- Mahmoudi, S., Bennour, A., Srasra, E., & Zargouni, F. (2016). Characterization, firing behavior and ceramic application of clays from the Gabes region in South Tunisia. *Applied Clay Science*, 135, 215–225. <https://doi.org/10.1016/j.clay.2016.09.023>
- Manfredini, T., & Hanuskova, M. (2012). Natural raw materials in “traditional” ceramic manufacturing. *Journal of the University of Chemical Technology and Metallurgy*, 47(4), 465–470.
- Manni, A., Elhaddar, A., El Bouari, A., El Hassani, E. A., & Sadik, C. (2017). Complete characterization of Berrechid clays (Morocco) and manufacturing of new ceramic using minimal amounts of feldspars: Economic implication. *Case Studies in Construction Materials*, 7(April), 144–153. <https://doi.org/10.1016/j.cscm.2017.07.001>
- Martín-Márquez, J., De La Torre, A. G., Aranda, M. A. G., Rincón, J. M., & Romero, M. (2009). Evolution with temperature of crystalline and amorphous phases in porcelain stoneware. *Journal of the American Ceramic Society*, 92(1), 229–234. <https://doi.org/10.1111/j.1551-2916.2008.02862.x>
- McManus, J. (1988). Grain size determination and interpretation. *EurekaMag*, 63–85 <https://eurekamag.com/research/019/094/019094940.php>
- Mehta, N. S., Sahu, P. K., Tripathi, P., Pyare, R., & Majhi, M. R. (2018). Influence of alumina and silica addition on the physico-mechanical and dielectric behavior of ceramic porcelain insulator at high sintering temperature. *Boletín de la Sociedad Española de Cerámica y Vidrio*, 57(4), 151–159. <https://doi.org/10.1016/j.bsecev.2017.11.002>
- Meng, Y., Gong, G., Wu, Z. P., Yin, Z. J., Xie, Y. M., & Liu, S. R. (2012). Fabrication and microstructure investigation of ultra-high-strength porcelain insulator. *Journal of the European Ceramic Society*, 32, 3043–3049. <https://doi.org/10.1016/j.jeurceramsoc.2012.04.015>
- Mercury, J. M. R., Cabral, A. A., Paiva, A. E. M., Angélica, R. S., Neves, R. F., & Scheller, T. (2011). Thermal behavior

- and evolution of the mineral phases of Brazilian red mud. *Journal of Thermal Analysis and Calorimetry*, 104(2), 635–643. <https://doi.org/10.1007/s10973-010-1039-7>
- Merga, A., Murthy, H., Amare, E., Ahmed, K., & Bekele, E. (2019). Fabrication of electrical porcelain insulator from ceramic raw materials of Oromia region, Ethiopia. *Heliyon*, 5. <https://doi.org/10.1016/j.heliyon.2019.e02327>
- Moraes, J. D. D., Bertolino, S. R. A., Cuffini, S. L., Ducart, D. F., Bretzke, P. E., & Leonardi, G. R. (2017). Clay minerals: Properties and applications to dermocosmetic products and perspectives of natural raw materials for therapeutic purposes—A review. *International Journal of Pharmaceutics*, 534(1–2), 213–219. <https://doi.org/10.1016/j.ijpharm.2017.10.031>
- Morkel, J., & Vermaak, M. K. G. (2006). The role of swelling clay in kimberlite weathering. *Transactions of the Institutions of Mining and Metallurgy, Section C: Mineral Processing and Extractive Metallurgy*, 115(3), 150–154. <https://doi.org/10.1179/174328506X109121>
- Ngayakamo, B., & Eugene Park, S. (2019). Evaluation of kalamani vermiculite for production of high strength porcelain insulators. *Science of Sintering*, 51(2), 1–10. <https://doi.org/10.2298/SOS1902223N>
- Ngayakamo, B., & Park, S. E. (2018a). Effect of firing temperature on triaxial electrical porcelain properties made from Tanzania locally sourced ceramic raw materials. *Epitoanyag - Journal of Silicate Based and Composite Materials*, 70(4), 106–109. <https://doi.org/10.14382/epitoanyag-jsbcm.2018.19>
- Ngayakamo, B., & Park, S. E. (2018b). Evaluation of Tanzania local ceramic raw materials for high voltage porcelain insulators production. *Ceramica*, 64, 570–576. <https://doi.org/10.1590/0366-69132018643722427>
- Nwachukwu, V. C., & Lawal, S. A. (2018). Investigating the production quality of electrical porcelain insulators from local materials. *IOP Conference Series: Materials Science and Engineering*, 413, 1–9. <https://doi.org/10.1088/1757-899X/413/1/012076>
- Ochen, W. (2019). Effect of quartz particle size on sintering behavior and flexural strength of porcelain tiles made from raw materials in Uganda. *Advances in Materials*, 8, 33. <https://doi.org/10.11648/j.am.20190801.15>
- Ologunwa, T., Akinbogun, T., Frischer, R., Kashim, I., Kuca, K., Krejcar, O., & Fadeyi, O. (2021). Optimizing performance of porcelain insulators: How does particle size influence dielectric and mechanical strengths? *Acta Mechanica Slovaca*, 25(2), 20–28. <https://doi.org/10.21496/ams.2021.017>
- Olupot, P. W., Jonsson, S., & Byaruhanga, J. K. (2010). Development and characterisation of triaxial electrical porcelains from Ugandan ceramic minerals. *Ceramics International*, 36(4), 1455–1461. <https://doi.org/10.1016/j.ceramint.2010.02.006>
- Regassa, A., Van Daele, K., De Paepe, P., Dumona, M., Deckers, J., Asrat, A., & Van Ranst, E. (2014). Characterizing weathering intensity and trends of geological materials in the Gilgel gibe catchment, southwestern Ethiopia. *Journal of African Earth Sciences*, 99(PA2), 568–580. <https://doi.org/10.1016/j.jafrearsci.2014.05.012>
- Roy, S., & Kumar Bhalla, S. (2017). Role of geotechnical properties of soil on civil engineering structures. *Resources and Environment*, 7(4), 103–109.
- Salihu, S., & Suleiman, I. (2018). Comparative analysis of physical and chemical characteristics of selected clays deposits found in Kebbi state, Nigeria. *International Journal of Physical Sciences*, 13(10), 163–173.
- Sánchez-Soto, P. J., Eliche-Quesada, D., Martínez-Martínez, S., Garzón-Garzón, E., Pérez-Villarejo, L., & Rincón, J. M. (2018). The effect of vitreous phase on mullite and mullite-based ceramic composites from kaolin wastes as by-products of mining, sericite clays and kaolinite. *Materials Letters*, 223, 154–158. <https://doi.org/10.1016/j.matlet.2018.04.037>
- Schettino, M. A. S., Siqueira, F. B., & Holanda, J. N. F. (2016). Densification behavior of floor tiles added with sugarcane bagasse ash waste. *Ciência & Tecnologia Dos Materiais*, 28(1), 60–66. <https://doi.org/10.1016/j.ctmat.2015.10.004>
- Souza, A. E., Teixeira, S. R., Santos, G. T. A., Costa, F. B., & Longo, E. (2011). Reuse of sugarcane bagasse ash (SCBA) to produce ceramic materials. *Journal of Environmental Management*, 92(10), 2774–2780. <https://doi.org/10.1016/j.jenvman.2011.06.020>
- Tang, Q., Wang, F., Tang, M., Liang, J., & Ren, C. (2012). Study on pore distribution and formation rule of sepiolite mineral nanomaterials. *Journal of Nanomaterials*, 2012. <https://doi.org/10.1155/2012/382603>
- Teixeira, S. R., De Souza, A. E., De Almeida Santos, G. T., Peña, A. F. V., & Miguel, Á. G. (2008). Sugarcane bagasse ash as a potential quartz replacement in red ceramic. *Journal of the American Ceramic Society*, 91(6), 1883–1887. <https://doi.org/10.1111/j.1551-2916.2007.02212.x>
- Trindade, M. J., Dias, M. I., Coroado, J., & Rocha, F. (2010). Firing tests on clay-rich raw materials from the Algarve basin (southern Portugal): Study of mineral transformations with temperature. *Clays and Clay Minerals*, 58(2), 188–204. <https://doi.org/10.1346/CCMN.2010.0580205>
- Tsozué, D., Nzeugang, A. N., Mache, J. R., Loweh, S., & Fagel, N. (2017). Mineralogical, physico-chemical and technological characterization of clays from Maroua (far-north, Cameroon) for use in ceramic bricks production. *Journal of Building Engineering*, 11(March), 17–24. <https://doi.org/10.1016/j.job.2017.03.008>
- Valášková, M. (2015). Clays, clay minerals and cordierite ceramics – A review. *Ceramics Silikaty*, 59, 331–340.
- Velde, B., & Meunier, A. (2008). *The origin of clay minerals in soils and weathered rocks* (Vol. Issue 1). In *Springer Science & Business Media*. <https://doi.org/10.1007/978-3-540-75634-7>.
- Yaya, A., Tiburu, E. K., Vickers, M. E., Efavi, J. K., Onwona-Agyeman, B., & Knowles, K. M. (2017). Characterisation and identification of local kaolin clay from Ghana: A potential material for electroporcelain insulator fabrication. *Applied Clay Science*, 150, 125–130. <https://doi.org/10.1016/j.clay.2017.09.015>
- Zbik, M. S., Martens, W. N., Frost, R. L., Song, Y. F., Chen, Y. M., Chen, J., & h. (2010). Smectite flocculation structure modified by Al13 macro-molecules - as revealed by transmission X-ray microscopy (TXM). *Journal of Colloid and Interface Science*, 345(1), 34–40. <https://doi.org/10.1016/j.jcis.2010.01.043>

Springer Nature or its licensor (e.g. a society or other partner) holds exclusive rights to this article under a publishing agreement with the author(s) or other rightsholder(s); author self-archiving of the accepted manuscript version of this article is solely governed by the terms of such publishing agreement and applicable law.